Strong Intrinsic Spin Hall Effect in the TaAs Family of Weyl Semimetals

Yan Sun,[1] Yang Zhang,[1,2] Claudia Felser,[1] and Binghai Yan[1,3,*]
[1]Max Planck Institute for Chemical Physics of Solids, 01187 Dresden, Germany
[2]Leibniz Institute for Solid State and Materials Research, 01069 Dresden, Germany
[3]Max Planck Institute for the Physics of Complex Systems, 01187 Dresden, Germany
(Received 27 April 2016; revised manuscript received 29 August 2016; published 30 September 2016)

Since their discovery, topological insulators are expected to be ideal spintronic materials owing to the spin currents carried by surface states with spin-momentum locking. However, the bulk doping problem remains an obstacle that hinders such an application. In this work, we predict that a newly discovered family of topological materials, the Weyl semimetals, exhibits a large intrinsic spin Hall effect that can be utilized to generate and detect spin currents. Our *ab initio* calculations reveal a large spin Hall conductivity in the TaAs family of Weyl materials. Considering the low charge conductivity of semimetals, Weyl semimetals are believed to present a larger spin Hall angle (the ratio of the spin Hall conductivity over the charge conductivity) than that of conventional spin Hall systems such as the 4*d* and 5*d* transition metals. The spin Hall effect originates intrinsically from the bulk band structure of Weyl semimetals, which exhibit a large Berry curvature and spin-orbit coupling, so the bulk carrier problem in the topological insulators is naturally avoided. Our work not only paves the way for employing Weyl semimetals in spintronics, but also proposes a new guideline for searching for the spin Hall effect in various topological materials.

DOI: 10.1103/PhysRevLett.117.146403

Topological insulators (TIs) are characterized by metallic surface states inside the bulk energy gap [1,2], in which the spin and momentum are locked together with a vortexlike spin texture. Because counterpropagating surface states carry opposite spins, if a charge current is introduced into a nominally perfect TI (with no bulk conductivity), the current should be fully spin polarized. Thus, TIs have been considered as excellent materials for generating a spin current, and this expectation has stimulated several recent experimental studies of the spin Hall effect (SHE) in TIs such as Bi_2Se_3 [3] and $(Bi_{0.5}Sb_{0.5})_2Te_3$ [4] that demonstrated highly efficient spin current conversion. However, the unavoidable bulk carrier problem remains an obstacle to the widespread application of TIs. Interestingly, an exotic type of topological semimetal, the Weyl semimetal (WSM), exhibits similar spin-momentum locking in both the bulk and topological surface states [5–9]. Therefore, we are motivated to study the SHE, which refers to transverse spin current generation by a longitudinal charge current and is essential for state-of-the-art spintronic applications [10], in this new family of topological materials.

In a WSM, the conduction and valence bands cross each other linearly in the three-dimensional (3D) momentum space near the Fermi energy through nodal points, called Weyl points, in a 3D analog of the band structure of graphene. Because of the strong spin-orbit coupling (SOC), the Weyl points act as sources or sinks of the Berry curvature [11], which characterizes the entanglement between the conduction and valence bands. Here, we naturally expect the existence of a large SHE intrinsically originating from the bulk band structure, because the SHE is derived from the spin-momentum locking and Berry curvature of the electronic bands [12,13]. Recently, the first family of WSMs was predicted [14,15] and discovered by angle-resolved photoemission spectroscopy [16–19] in the transition-metal pnictides TaAs, TaP, NbAs, and NbP (and also in photonic crystals [20]). Further, much effort has been devoted to determining their transport properties, such as the chiral anomaly effect [21–24] and extremely large magnetoresistance [25,26].

In this work, we investigated the intrinsic SHE of the TaAs family of WSMs by *ab initio* calculations and indeed observed a large spin Hall conductivity (SHC), which originates from the nodal-line-like band anticrossing near the Fermi energy. The SHC is anisotropic, suggesting that the crystallographic *ab* surface is the favored plane for setting up the orthogonal charge and spin currents in experiments. Because the SHE of WSMs originates from the bulk electronic states rather than the surface states, WSMs do not exhibit the bulk doping problem that affects TI materials. Therefore, we argue that WSMs may be superior to TIs for SHE devices, as we demonstrate a strong SHE in WSMs.

Density-functional theory calculations within the generalized gradient approximation [27,28] were carried out for the bulk compounds. The *ab initio* density-functional theory wave functions were projected to atomic-orbital-like Wannier functions [29], based on which we constructed an effective Hamiltonian $\hat{H}$ in a tight-binding scheme. We note that Wannier functions were well optimized, so that the effective Hamiltonian fully respects the symmetry of corresponding materials, which is crucial to compute the SHE. Using the above material-specific effective Hamiltonian, we employed the Kubo formula approach at the clean limit [12,13] to calculate the SHC

$$\sigma_{ij}^{k} = e\hbar \int_{BZ} \frac{d\vec{k}}{(2\pi)^3} \sum_{n} f_{n\vec{k}} \Omega_{n,ij}^{k}(\vec{k}),$$

$$\Omega_{n,ij}^{s,k}(\vec{k}) = -2\mathrm{Im} \sum_{n' \neq n} \frac{\langle n\vec{k}|\hat{J}_i^k|n'\vec{k}\rangle\langle n'\vec{k}|\hat{v}_j|n\vec{k}\rangle}{(E_{n\vec{k}} - E_{n'\vec{k}})^2}, \quad (1)$$

where the spin current operator $\hat{J}_i^k = \frac{1}{2}\{\hat{v}_i, \hat{s}_k\}$ with the spin operator $\hat{s}$ and velocity operator $\hat{v}_i = (1/\hbar)(\partial\hat{H}/\partial k_i)$ and $i, j, k = x, y, z$. Further, $|n\vec{k}\rangle$ and $E_{n\vec{k}}$ are the eigenvector and eigenvalue of the Hamiltonian $\hat{H}$, respectively. $\Omega_{n,ij}^{s,k}(\vec{k})$ is referred to as the spin Berry curvature, for which the ordinary Berry curvature $\Omega_{n,ij}(\vec{k})$ can be obtained by substituting the velocity operator $\hat{v}_i$ for $\hat{J}_i^k$. In a system where s_z is a good quantum number, it is simple to understand the correlation between spin Berry curvature and its ordinary counterpart, $\Omega_{n,xy}^{s,z} = s_z \Omega_{n,xy}(\vec{k})$. The temperature dependence is included in the Fermi-Dirac distribution $f_{n\vec{k}}$. From Eq. (1) one can see that the SHC $\sigma_{ij}^{k}(\mu)$ is a third-order tensor and represents the spin current $(j_i^{s,k})$ along the ith direction generated by an electric field (E_j) along the jth direction, where the spin current is polarized along the kth direction, μ is the Fermi energy, and $j_i^{s,k} = \sigma_{ij}^{k}(\mu) E_j$. For the integral in Eq. (1), a dense grid of $500 \times 500 \times 500$ was adopted in the first Brillouin zone for the convergence of SHC values. More information about the methods is in Ref. [30].

We first demonstrate the SHE in two simple systems by effective model Hamiltonians, the quantum spin Hall effect (QSHE) insulator and the Weyl semimetal. For the QSHE, the well-known Bernevig-Hughes-Zhang model [32] was considered, where s_z is preserved as a good quantum number. We can simply compute its SHC by Eq. (1). According to the Bernevig-Hughes-Zhang model, the conduction and valence band get inverted near the Brillouin zone center, where the band touching points form a nodal line [see Fig. 1(a)]. Without including SOC, the SHC is zero. As long as the SOC is turned on, the nodal line is fully gapped out and a nonzero SHC (σ_{yx}^{z}) appears spontaneously. In the two-dimensional (2D) Brillouin zone, the SHC is dominantly contributed by the band anticrossing region near the original nodal line, as shown in Fig. 1(b). When the Fermi energy μ lies in the energy gap where there is no Fermi surface, the SHC is purely a topological quantity with a quantized value $G_0(\hbar/2e)$, where $G_0 = (2e^2/h)$ is the conductance quantum and $(\hbar/2e)$ is the unit converting from charge current to spin current. As long as μ starts merging into conduction or valence bands, the SHC decreases due to the Fermi surface contribution. From the 2D QSHE to the 3D TI, the SHC is still related to the band anticrossing, but not necessarily quantized any more.

For a 3D WSM, we adopt a minimal Hamiltonian in a two-band model [30,33], where s_z is preserved and only a single pair of Weyl points appears at $\pm k_W$ of the k_z axis. When Fermi energy crosses the Weyl points, the Berry flux between this pair of Weyl points leads to a noninteger anomalous Hall conductivity (AHC) $\sigma_{yx}^{\mathrm{AH}} = -(k_W/\pi)(e^2/h)$, which is proportional to the Weyl point separation and reported in Refs. [34,35]. Such an anomalous Hall effect current simply carries a spin current, since

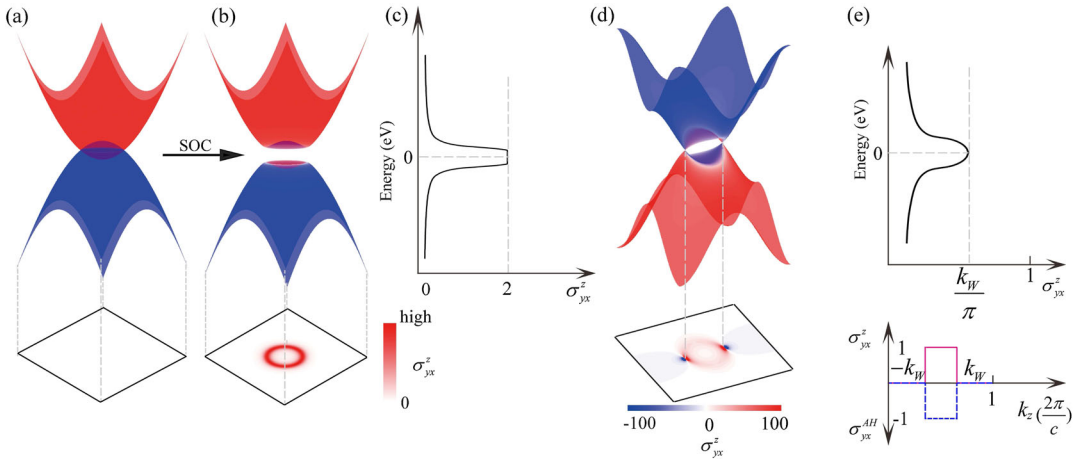

FIG. 1. Spin Hall effect in a quantum spin Hall insulator and a Weyl semimetal based on simple analytical models. In a QSHE, the valence and conduction bands get inverted (a) and SOC opens an energy gap at the nodal-ring band crossing points (b). (c) The resultant SHC is quantized inside the energy gap, which is mainly contributed by the nodal-ring area of the band structure. (d) Energy dispersion in the $k_y = 0$ plane for the WSM and the corresponding spin Berry curvature distribution with the chemical potential crossing at the Weyl points. (e) The upper panel is the energy dependent SHC for the WSM, where the maximum value appears at the the Weyl points. And the lower panel is the k_z dependent SHC (σ_{yx}^{z}, red line) and AHC ($\sigma_{yx}^{\mathrm{AH}}$, dashed blue line) integrated in the $k_x k_y$ plane. The nonzero quantized SHC and AHC only exist between these two Weyl points. The color bars in (b) and (d) are in arbitrary units. The units for the AHC and SHC are (e^2/h) and $(e^2/h)(\hbar/2e)$, respectively.

the system is spin polarized. Therefore, we can easily conclude that the corresponding SHC is

$$\sigma_{yx}^{z} = -\frac{s_z}{e}\sigma_{yx}^{\mathrm{AH}} = -\frac{\hbar}{2e}\sigma_{yx}^{\mathrm{AH}}, \tag{2}$$

where the "−" sign is due to the negative charge of the electrons. This is further verified by our numerical calculations using Eq. (1). Near a single Weyl point, the spin Berry curvature shows a p-orbital-like distribution with the Weyl point being the node, as shown in Fig. 1(d), which can be understood by projecting the monopolelike Berry curvature to the s_z axis. Here, the SHC is even under the time reversal operation at the Weyl point in energy. If a WSM preserves the time-reversal symmetry, the anomalous Hall effect disappears while the SHE can still survive, because the SHE is even under the time reversal.

Further, we investigate the SHE in specific materials. The crystal structure of the TaAs family of compounds belongs to the noncentrosymmetric tetragonal lattice (space group $I4_1md$, No. 109). Thus, the corresponding SHE is anisotropic on the basis of the linear response. The existing symmetries in the material, such as time-reversal symmetry and mirror reflections, force many tensor elements to be zero or equivalent [36,37], leaving only three groups of nonzero elements, $\sigma_{xy}^{z} = -\sigma_{yx}^{z}$, $\sigma_{zx}^{y} = -\sigma_{zy}^{x}$, and $\sigma_{yz}^{x} = -\sigma_{xz}^{y}$.

Table I shows the calculated SHC for four WSM compounds TaAs, TaP, NbAs, and NbP, in which the Fermi energy lies at the electron-hole compensation (charge neutral) point and the temperature is 0 K. From right to left, the amplitude of the SHC increases quickly for a given SHC element, which is consistent with the increasing trend of SOC for these four compounds [19,38]. For a given compound (except NbP), σ_{xy}^{z} is much larger than the corresponding σ_{zx}^{y} and σ_{yz}^{x}. This indicates that the optimal setup to exploit the large SHC is to have charge and spin currents lying inside the xy plane (i.e., ab plane), for example, a charge current along the x direction and a spin current along the y direction. Up to room temperature, we found that the SHC reduces only slightly up to the room temperature, which is consistent with the weak temperature dependence of the intrinsic SHE [12].

TABLE I. Nonzero tensor elements of the spin Hall conductivity for four WSM compounds. The Fermi energy is set to the charge neutral point, which is very close to the real chemical potential in materials. The spin Hall conductivity is in units of $(\hbar/e)(\Omega\,\mathrm{cm})^{-1}$.

	TaAs	TaP	NbAs	NbP
σ_{xy}^{z}	−781	−603	−330	7
σ_{zx}^{y}	−382	−437	−312	−83
σ_{yz}^{x}	−357	−344	−260	−135

The large amplitudes of the SHC [e.g., $\sigma_{xy}^{z} = -781\ (\hbar/e)(\Omega\,\mathrm{cm})^{-1}$ for TaAs] are comparable to the values for ordinary $4d$ and $5d$ transition metals [39,40]. A key criterion to benchmark a SHE material is the large spin Hall angle, the ratio of the SHC over the charge conductivity, which characterizes the efficiency of converting the charge current to a spin current. Compared to Pt [39], the SHC of TaAs-family WSMs is still several times smaller. However, it is reasonable to presume that the charge conductivity of these semimetals is orders of magnitude smaller than that of the metal Pt, when they are all in the thin-film form to fabricate SHE devices. Thus, we expect that the spin Hall angle of these WSMs can be even larger than that of Pt. In addition to the large spin-Hall conductivity, the spin lifetime and spin diffusion length are also essential ingredients for device applications, which is beyond our current calculations. Considering the large electron mean free path observed in transport (e.g., 0.4 μm for TaP [24]), one may obtain a long spin diffusion length in these WSMs as well.

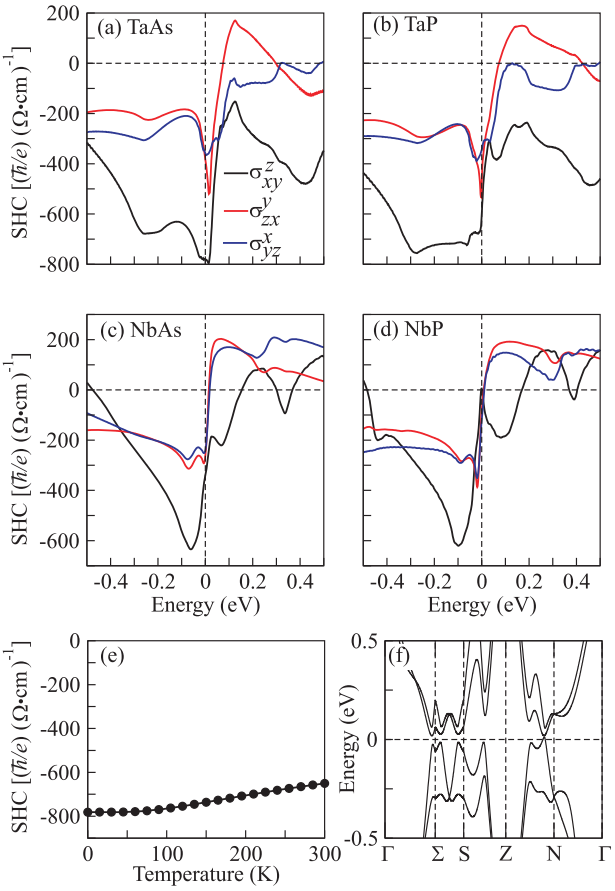

FIG. 2. Energy-dependent spin Hall conductivity tensor elements (σ_{xy}^{z}, σ_{zx}^{y}, and σ_{yz}^{x}) for (a) TaAs, (b) TaP, (c) NbAs, and (d) NbP. The Fermi energy is set to zero at the charge neutral point. (e) The temperature-dependent SHC for TaAs. (f) For completeness, the energy dispersion is shown.

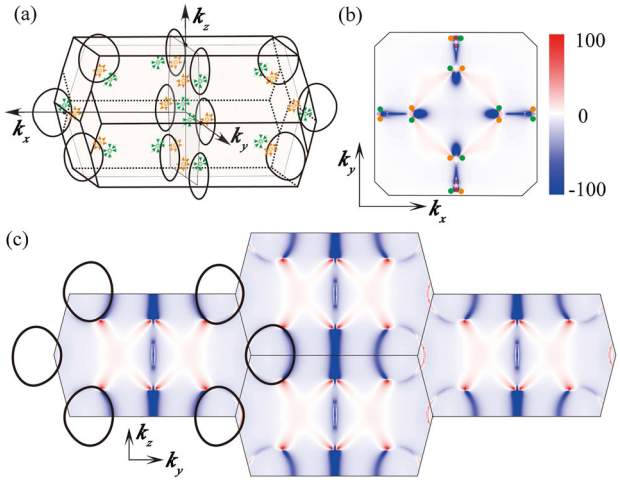

FIG. 3. Spin Berry curvature in the Brillouin zone. (a) First Brillouin zone of TaAs. The black circles represent nodal line loops, and the green and yellow points represent Weyl points with opposite chirality. The nodal lines lie in the mirror planes, which are shown in gray. (b) Spin Berry curvature projected to the $k_x k_y$ plane. The green and yellow points represent the positions of the projected Weyl points with opposite chirality. (c) Spin Berry curvature projected to the $k_y k_z$ plane. The black loops indicate nodal lines. One can find that the spin Hall conductivity arises mainly from the energy bands around the nodal lines. The color bar is in arbitrary units.

Because the SHC depends on the Fermi energy [see Eq. (1)], it varies quickly when the Fermi energy is shifted below or above the charge neutral point. As shown in Fig. 2, the σ_{xy}^{z} values of NbAs and NbP can reach the maximal amplitude of about 600 $(\hbar/e)(\Omega\,\mathrm{cm})^{-1}$ when the Fermi energy lies at -0.1 eV. A slight downshift of the Fermi energy can also increase the σ_{xy}^{z} value of TaP to around 700 $(\hbar/e)(\Omega\,\mathrm{cm})^{-1}$. In contrast, the maximal σ_{xy}^{z} value appears almost at the electron-hole compensation point for TaAs. The energy-dependent analysis indicates the general route to optimizing the SHE in these materials.

The SHC exhibits peak values near the charge neutral point, which is close to the Weyl points in energy. It is known that the crossing points between the conduction and valence bands form nodal line loops in the mirror planes of the Brillouin zone without SOC. When SOC is included, the nodal lines are gapped out, leaving only special gapless points, i.e., Weyl points, which are located near the original nodal lines but away from the mirror planes. Because of the lack of a whole indirect energy gap, the Fermi energy still crosses some conduction and valence bands near the nodal lines, as revealed in previous theoretical and experimental studies [24,26,41]. Taking σ_{xy}^{z} for TaAs as an example, the corresponding spin Berry curvatures are shown in Figs. 3(b) and 3(c) by projecting them onto the $k_x k_y$ and $k_y k_z$ planes, respectively. One can find that the dominant amplitude of the spin Berry curvature (blue regions) is distributed mainly around the nodal line area. This is consistent with in the quantum spin Hall effect (see Fig. 1), where the band anticrossing contributes a large SHC. Further, we speculate that a large SHE will also exist in other topological materials, especially those with nodal-point and nodal-line-like Fermi surfaces and strong SOC [7,42–49]. When the Fermi energy crosses the Weyl points, the spin Berry curvature exhibits a p-orbital-like spatial distribution, very similar to the observation for the simple two-band model (see Fig. 1 and Ref. [30]), which is determined by the monopole feature of Berry curvature near the Weyl point.

In summary, we theoretically predicted a strong SHE in the TaAs family of Weyl semimetals. The nodal-line-like Fermi surface was found to contribute to a large SHC, where both trivial and Weyl pockets exist. Even though the Weyl pockets diminish when the Fermi energy is sufficiently close to the Weyl points, we still found an intrinsic contribution to the SHC from the Weyl points as a pure topological effect. Our findings regarding this family of WSMs can also be generalized to other topological materials such as Dirac and nodal line semimetals.

We thank Stuart S. P. Parkin, Shun-Qing Shen, Jeroen van den Brink, and Zhong-Kai Liu for helpful discussions. B. Y. specially acknowledges the inspiring remarks by B. Andrei Bernevig and Jairo Sinova during the SPICE Young Research Leader Workshop. We thank the Shanghai Supercomputer Center. This work was financially supported by the ERC (Advanced Grant No. 291472 "Idea Heusler") and the German Research Foundation (DFG) (SFB-1143 and SPP-1666/YA328/5-1).

*yan@cpfs.mpg.de

[1] X.-L. Qi and S.-C. Zhang, Rev. Mod. Phys. **83**, 1057 (2011).
[2] M. Z. Hasan and C. L. Kane, Rev. Mod. Phys. **82**, 3045 (2010).
[3] A. R. Mellnik, J. S. Lee, A. Richardella, J. L. Grab, P. J. Mintun, M. H. Fischer, A. Vaezi, A. Manchon, E. A. Kim, N. Samarth, and D. C. Ralph, Nature (London) **511**, 449 (2014).
[4] Y. Fan, P. Upadhyaya, X. Kou, M. Lang, S. Takei, Z. Wang, J. Tang, L. He, L.-T. Chang, M. Montazeri, G. Yu, W. Jiang, T. Nie, R. N. Schwartz, Y. Tserkovnyak, and K. L. Wang, Nat. Mater. **13**, 699 (2014).
[5] X. G. Wan, A. M. Turner, A. Vishwanath, and S. Y. Savrasov, Phys. Rev. B **83**, 205101 (2011).
[6] L. Balents, Physics **4**, 36 (2011).
[7] A. A. Burkov, M. D. Hook, and L. Balents, Phys. Rev. B **84**, 235126 (2011).
[8] P. Hosur and X. L. Qi, C.R. Phys. **14**, 857 (2013).
[9] O. Vafek and A. Vishwanath, Annu. Rev. Condens. Matter Phys. **5**, 83 (2014).
[10] T. Jungwirth, J. Wunderlich, and K. Olejník, Nat. Mater. **11**, 382 (2012).
[11] G. E. Volovik, *The Universe in A Helium Droplet* (publisher Clarendon Press, Oxford, 2003).

[12] J. Sinova, S. O. Valenzuela, J. Wunderlich, C. Back, and T. Jungwirth, Rev. Mod. Phys. **87**, 1213 (2015).
[13] D. Xiao, M.-C. Chang, and Q. Niu, Rev. Mod. Phys. **82**, 1959 (2010).
[14] H. Weng, C. Fang, Z. Fang, B. A. Bernevig, and X. Dai, Phys. Rev. X **5**, 011029 (2015).
[15] S.-M. Huang, S.-Y. Xu, I. Belopolski, C.-C. Lee, G. Chang, B. Wang, N. Alidoust, G. Bian, M. Neupane, C. Zhang, S. Jia, A. Bansil, H. Lin, and M. Z. Hasan, Nat. Commun. **6**, 8373 (2015).
[16] S.-Y. Xu, I. Belopolski, N. Alidoust, M. Neupane, G. Bian, C. Zhang, R. Sankar, G. Chang, Y. Zhujun, C.-C. Lee, H. Shin-Ming, H. Zheng, J. Ma, D. S. Sanchez, B. Wang, A. Bansil, F. Chou, P. P. Shibayev, H. Lin, S. Jia, and M. Z. Hasan, Science **349**, 613 (2015).
[17] B. Q. Lv, H. M. Weng, B. B. Fu, X. P. Wang, H. Miao, J. Ma, P. Richard, X. C. Huang, L. X. Zhao, G. F. Chen, Z. Fang, X. Dai, T. Qian, and H. Ding, Phys. Rev. X **5**, 031013 (2015).
[18] L. X. Yang, Z. K. Liu, Y. Sun, H. Peng, H. F. Yang, T. Zhang, B. Zhou, Y. Zhang, Y. F. Guo, M. Rahn, D. Prabhakaran, Z. Hussain, S. K. Mo, C. Felser, B. Yan, and Y. L. Chen, Nat. Phys. **11**, 728 (2015).
[19] Z. K. Liu, L. X. Yang, Y. Sun, T. Zhang, H. Peng, H. F. Yang, C. Chen, Y. Zhang, Y. F. Guo, D. Prabhakaran, M. Schmidt, Z. Hussain, S.-K. Mo, C. Felser, B. Yan, and Y. L. Chen, Nat. Mater. **15**, 27 (2016).
[20] L. Lu, Z. Wang, D. Ye, L. Ran, L. Fu, J. D. Joannopoulos, and M. Soljačić, Science **349**, 622 (2015).
[21] J. Xiong, S. K. Kushwaha, T. Liang, J. W. Krizan, M. Hirschberger, W. Wang, R. J. Cava, and N. P. Ong, Science **350**, 413 (2015).
[22] X. Huang, L. Zhao, Y. Long, P. Wang, D. Chen, Z. Yang, H. Liang, M. Xue, H. Weng, Z. Fang, X. Dai, and G. Chen, Phys. Rev. X **5**, 031023 (2015).
[23] C.-L. Zhang*et al.*, Nat. Commun. **7**, 10735 (2016).
[24] F. Arnold, C. Shekhar, S.-C. Wu, Y. Sun, R. D. dos Reis, N. Kumar, M. Naumann, M. O. Ajeesh, M. Schmidt, A. G. Grushin, J. H. Bardarson, M. Baenitz, D. Sokolov, H. Borrmann, M. Nicklas, C. Felser, E. Hassinger, and B. Yan, Nat. Commun. **7**, 11615 (2016).
[25] C. Shekhar, A. K. Nayak, Y. Sun, M. Schmidt, M. Nicklas, I. Leermakers, U. Zeitler, Y. Skourski, J. Wosnitza, Z. Liu, Y. Chen, W. Schnelle, H. Borrmann, Y. Grin, C. Felser, and B. Yan, Nat. Phys. **11**, 645 (2015).
[26] J. Klotz, S.-C. Wu, C. Shekhar, Y. Sun, M. Schmidt, M. Nicklas, M. Baenitz, M. Uhlarz, J. Wosnitza, C. Felser, and B. Yan, Phys. Rev. B **93**, 121105 (2016).
[27] J. P. Perdew, K. Burke, and M. Ernzerhof, Phys. Rev. Lett. **77**, 3865 (1996).
[28] G. Kresse and J. Furthmüller, Phys. Rev. B **54**, 11169 (1996).
[29] A. A. Mostofi, J. R. Yates, Y.-S. Lee, I. Souza, D. Vanderbilt, and N. Marzari, Comput. Phys. Commun. **178**, 685 (2008).
[30] See Supplemental Material at http://link.aps.org/supplemental/10.1103/PhysRevLett.117.146403 for more details of the model Hamiltonians, calculation methods, and results. References [27–29,31–33] are included in the Supplemental Material.
[31] J.-O. Willerstrom, J. Less-Common Met. **99**, 273, (1984).
[32] B. A. Bernevig, T. L. Hughes, and S.-C. Z. Zhang, Science **314**, 1757 (2006).
[33] H.-Z. Lu, S.-B. Zhang, and S.-Q. Shen, Phys. Rev. B **92**, 045203 (2015).
[34] K.-Y. Yang, Y.-M. Lu, and Y. Ran, Phys. Rev. B **84**, 075129 (2011).
[35] A. A. Burkov, Phys. Rev. Lett. **113**, 187202 (2014).
[36] W. H. Kleiner, Phys. Rev. **142**, 318 (1966).
[37] M. Seemann, D. Kodderitzsch, S. Wimmer, and H. Ebert, Phys. Rev. B **92**, 155138 (2015).
[38] Y. Sun, S. C. Wu, and B. Yan, Phys. Rev. B **92**, 115428 (2015).
[39] G. Y. Guo, S. Murakami, T.-W. Chen, and N. Nagaosa, Phys. Rev. Lett. **100**, 096401 (2008).
[40] T. Tanaka, H. Kontani, M. Naito, T. Naito, D. S. Hirashima, K. Yamada, and J. Inoue, Phys. Rev. B **77**, 165117 (2008).
[41] F. Arnold, M. Naumann, S.-C. Wu, Y. Sun, M. Schmidt, H. Borrmann, C. Felser, B. Yan, and E. Hassinger, arXiv: 1603.08846.
[42] Z. Wang, Y. Sun, X.-Q. Chen, C. Franchini, G. Xu, H. Weng, X. Dai, and Z. Fang, Phys. Rev. B **85**, 195320, (2012).
[43] Z. K. Liu, B. Zhou, Y. Zhang, Z. J. Wang, H. M. Weng, D. Prabhakaran, S.-K. Mo, Z. X. Shen, Z. Fang, X. Dai, Z. Hussain, and Y. L. Chen, Science **343**, 864 (2014).
[44] C. Fang, Y. Chen, H.-Y. Kee, and L. Fu, Phys. Rev. B **92**, 081201 (2015).
[45] G. Bian *et al.*, Nat. Commun. **7**, 10556 (2016).
[46] Y. Wu, L.-L. Wang, E. Mun, D. D. Johnson, D. Mou, L. Huang, Y. Lee, S. L. Bud'ko, P. C. Canfield, and A. Kaminski, Nat. Phys. **12**, 667 (2016).
[47] L. M. Schoop, M. N. Ali, C. Straßer, V. Duppel, S. S. P. Parkin, B. V. Lotsch, and C. R. Ast, arXiv:1509.00861.
[48] A. A. Soluyanov, D. Gresch, Z. Wang, Q. Wu, M. Troyer, X. Dai, and B. A. Bernevig, Nature (London) **527**, 495 (2015).
[49] Y. Sun, S. C. Wu, M. N. Ali, C. Felser, and B. Yan, Phys. Rev. B **92**, 161107(R) (2015).